PAPER

Check for updates

Application of magnetic field to CO hydrogenation using a confined-space catalyst: effect on reactant gas diffusivity and reactivity

Waleeporn Donphai,[ab] Naphaphan Kunthakudee,[a] Sirapat Munpollasri,[ab] Pariyawalee Sangteantong,[ab] Surangrat Tonlublao,[c] Wanwisa Limphirat,[c] Yingyot Poo-arporn,[c] Sirapassorn Kiatphuengporn[d] and Metta Chareonpanich (ID) *[ab]

An external magnetic field has recently been applied in reaction processes to promote movement and avoid agglomeration of magnetic particles, and also reduce the activation energy through improving the gas–solid contact. In this work, the effect of an external magnetic field on reactant gas diffusivity and reactivity in CO hydrogenation within a confined-space catalyst was investigated for the first time using a conventional reactor packed with a bimetallic 5Fe–5Co/ZSM-5 molecular sieve catalyst. The synergistic effect between magnetic field and limited mass transfer within zeolite cavities improved the mass transfer ability and reaction phenomena of the reactant molecules, leading to enhancement of catalytic activity with tailored reaction pathways. As a result, CO conversion and CH_4 selectivity were increased by factors of 1.9 and 1.3 compared to those without a magnetic field. These synergistic interactions are able to provide an innovative challenge for green and sustainable chemical processes and separation processes by means of selective reactant and product mass transfer designed for selective catalytic conversion in the future.

Introduction

Carbon monoxide hydrogenation reactions have been explored and investigated by many researchers. Among these reactions, Fischer–Tropsch synthesis (FTS) is known as one important route for converting synthesis gas (CO and H_2) to high-quality and environmentally friendly hydrocarbon fuels.[1–3] To improve the conversion and selectivity for CO hydrogenation, suitable catalysts such as Fe and Co-based catalysts are generally applied. Fe-based catalysts show high activities for both the FTS reaction and water–gas shift (WGS) reaction, allowing for efficient utilization of CO,[4–6] while Co-based catalysts are superior at promoting long-chain hydrocarbons with low WGS activity at low operating temperatures.[7–9] In addition, catalyst supports also play crucial roles as regards various factors including cluster size of active metal particles,[5] mass transfer of reactants and products,[10] and chemisorption ratio of H_2 and CO on the active surfaces.[11] Among the catalyst supports, ZSM-5 zeolite exhibits superior performance in the CO hydrogenation reaction due to the confined spaces in the zeolite microstructure which help promote the re-adsorption ability and secondary reactions (*i.e.* cracking, isomerization, and aromatization) of the primary products, and possesses shape-selective features, leading to product selectivity towards gasoline-range hydrocarbons.[12–15]

In addition to the catalyst and support, various key parameters, such as reactant gas pressure, reaction temperature, and space velocity, also strongly influence the CO hydrogenation reaction. Recently, an external magnetic field has been applied for the first time in CO_2 reforming,[16] photocatalytic reaction,[17] Fischer–Tropsch synthesis,[18,19] hydrogen production,[20] in order to control and improve the movement of magnetic particles, avoid agglomeration of magnetic particles, and reduce the activation energy through improving gas–solid contact, respectively.[21–23] In previous work,[24–26] we fitted a catalytic packed bed reactor with an external magnetic field and observed significant improvement in CO_2 hydrogenation over Fe–Cu based catalysts by means of increased adsorption ability and selectivity to longer hydrocarbon products.

Accordingly, it is of a great interest to apply an external magnetic field to the CO hydrogenation reaction especially that in a conventional reactor packed with a confined-space bimetallic 5Fe–5Co/ZSM-5 catalyst. The mass transfer ability and reaction phenomena of reactant molecules are expected to be improved under magnetic field and magnified within a confined-space ZSM-5 molecular sieve, leading to

aKU-Green Catalysts Group, Department of Chemical Engineering, Faculty of Engineering, Kasetsart University, Bangkok 10900, Thailand. E-mail: fengmtc@ku.ac.th

bNanocatalysts and Nanomaterials for Sustainable Energy and Environment Research Network of NANOTEC, Kasetsart University, Bangkok 10900, Thailand

cSynchrotron Light Research Institute, Nakhon Ratchasima 30000, Thailand

dNational Nanotechnology Center, National Science and Technology Development Agency, Pathumthani 12120, Thailand

enhancement of catalytic activity with tailored reaction pathways. These synergistic interactions are able to provide an innovation challenge for simultaneous separation–reaction processes in the future.

Experimental

ZSM-5 zeolite and 5Fe–5Co/ZSM-5 catalyst preparation

ZSM-5 zeolite support was prepared following the synthesis process reported by Chareonpanich *et al.* (2018) using sodium silicate solution ($Na_2Si_3O_7$: 4 wt% NaOH; 27 wt% SiO_2) as a silica source, aluminium nitrate ($Al(NO_3)_3 \cdot 9H_2O$: 98% purity, UNILAB) as an alumina source and tetrapropyl ammonium bromide ($C_{12}H_{28}NBr$ or TPABr: 98% purity, Fluka Chemicals) as a structure-directing agent. Regarding the synthesis process, sodium silicate solution was primarily added into the mixture of TPABr and aluminium nitrate solution, while pH of the mixture was maintained at 10.5 throughout the mixing process by adding 1 M HCl solution. The mixture was kept stirring for 0.5 h and the obtained gel was transferred to a Teflon-lined autoclave and hydrothermally heated at 240 °C for 24 h. The solid product was filtered and washed with deionized water, dried at 80 °C for 24 h, and calcined in air at 550 °C for 4 h using a heating rate of 2 °C min^{-1} to remove TPABr and other volatile contaminants.

In this study, 5 wt% Fe and 5 wt% Co were loaded onto ZSM-5 zeolite support using iron nitrate ($Fe(NO_3)_3 \cdot 6H_2O$: 98%, Univar) and cobalt nitrate hexahydrate ($Co(NO_3)_2 \cdot 6H_2O$: 99.95%, Univar) as metal precursors *via* incipient wetness impregnation method. The obtained mixture was dried using microwave irradiation at 560 W for 2 min, and consecutively calcined in air at 500 °C for 5 h using a heating rate of 5 °C min^{-1}. The obtained catalyst was denoted as 5Fe–5Co/ZSM-5.

Characterization of textural, chemical, and magnetic properties of ZSM-5 zeolite and 5Fe–5Co/ZSM-5 catalyst

The textural properties of ZSM-5 zeolite support and 5Fe–5Co/ZSM-5 zeolite catalysts were examined by N_2 physisorption technique using a Quantachrome Autosorb-1C instrument at −196 °C. Prior to sorption measurement, the sample was degassed at 200 °C for 12 h. The specific surface area and pore size distribution were obtained by using Brunauer–Emmett–Teller (BET) analysis and *t*-plot method, and the pore volume was measured at a relative pressure of 0.995.

The crystallographic structures of ZSM-5 zeolite support and 5Fe–5Co/ZSM-5 catalyst were analyzed by X-ray diffraction spectroscopy (XRD: TTRAX III) using Cu Kα radiation at high angle in the 2θ range of 5–60°.

The surface morphology of ZSM-5 zeolite support and 5Fe–5Co/ZSM-5 catalyst were observed by using field emission scanning electron microscopy (FE-SEM: JEOL, JSM-7600F) operated at 15 keV with Pt-coated on the samples. Fe and Co elements on the catalyst surface were mapped by using energy-dispersive X-ray spectroscopy (EDS: OXFORD, XMaxN). The catalyst structure was examined by using transmission electron microscopy (TEM: JEOL JEM-2010) with an acceleration voltage of 200 kV.

The reducing temperatures of Fe and Co catalysts and interaction with ZSM-5 zeolite support were examined by using H_2 temperature programmed reduction (H_2-TPR: Micromeritics AutoChem II chemisorption analyzer). In the TPR experiment, 0.2 g of catalyst was heated in a flow of H_2/Ar mixture gas (10% H_2) using a total flow rate of 30 ml min^{-1}. The experiment was carried out in temperature range of 50–1000 °C with a heating rate of 5 °C min^{-1}.

Local geometry changes of Fe and Co species in catalyst during reduction stage with H_2 gas at a temperature range of 30–400 °C and holding stage of 400 °C for 6 h were investigated by time resolved X-ray absorption spectroscopy (TR-XAS) at Beamline 2.2 of the Synchrotron Light Research Institute (SLRI), Thailand. XANES spectra of Fe K-edge and Co K-edge were collected in energy ranges of 6975–7525 eV and 7690–7840 eV, respectively, in the transmission detection mode using ionization chamber.

Magnetic properties were measured using a vibrating sample magnetometer (VSM: Lake-Shore7404) with an external magnetic field of 5 kOe at room temperature.

Catalytic CO hydrogenation in external magnetic field

CO hydrogenation reaction over 5Fe–5Co/ZSM-5 zeolite catalyst was examined using a packed-bed reactor (SUS-316, O.D. 3/8″) assembled with a magnetic system (a ring cast Alnico permanent magnet: Bunting Magnetics Co. Ltd.; O.D., 1.0 in; I.D., 0.75 in; thickness, 0.5 in; grade 5) with a curie temperature of 840 °C and a maximum operating temperature of 538 °C. Magnetic field orientations (north to south (N–S) and south to north (S–N) alignments) and magnetic flux density at the catalyst bed were controlled by varying numbers of magnet pairs.

In this study, magnetic flux intensities at the catalyst bed were −20.8, −25.1 and −27.4 mT for two pairs, three pairs, and four pairs of magnets, respectively, with magnetic field orientation of N–S alignment. Prior to each experiment, 0.2 g catalyst packed at the center of magnet pairs was reduced at 400 °C for 6 h using a H_2 flow rate of 50 ml min^{-1} at atmospheric pressure. After catalyst activation, the reactor was cooled down to room temperature using He gas, then reactant gases (H_2 and CO with molar ratio of 2) were introduced into the reactor. The reaction was performed at 320 °C at a total pressure of 10 bar.

Effluent gases including H_2, CO, CO_2, and CH_4 were analyzed by using Shimadzu gas chromatograph (GC-2014) with a thermal conductivity detector (TCD) and a Unibead-C packed column, while hydrocarbon products (C_1–C_{5+}) were analyzed by Shimadzu gas chromatograph (GC-8A) with a flame ionization detector (FID). A Porapak-Q packed column and OV-1 Uniport HP packed column were used to analyze C_1–C_4 and C_{5+} hydrocarbons, respectively. Activity and selectivity of 5Fe–5Co/ZSM-5 catalyst without an external magnetic field were also examined in comparison.

Results and discussion

In this work, use of an external magnetic field and confined-space 5Fe–5Co/ZSM-5 catalyst reactant gas diffusivity and

catalytic reactivity in CO hydrogenation reaction were systematically investigated. Accordingly, ZSM-5 zeolite was prepared by hydrothermal synthesis, followed by loading of the active metals *via* incipient wetness impregnation method. The crystalline structures of ZSM-5 support and 5Fe–5Co/ZSM-5 catalyst were examined by X-ray diffraction spectroscopy (Fig. 1). The diffraction peaks of both ZSM-5 and 5Fe–5Co/ZSM-5 catalyst corresponded well to the MFI-type framework,[27,28] indicating good dispersion of Fe_2O_3 and CuO over ZSM-5 support. The specific surface areas of ZSM-5 support and 5Fe–5Co/ZSM-5 catalyst were found to be 271 and 227 m^2 g^{-1}, respectively, representing a type I isotherm with H4 hysteresis loop according to IUPAC classification (Fig. 2)—indicating the existence of a microporous structure with narrow slit pores. Pore size distribution of ZSM-5 zeolite was in the range of 0.3–0.7 nm, with a maximum of 0.6 nm, while a narrower pore was observed for 5Fe–5Co/ZSM-5 catalyst (0.4 nm). The fraction of micropore volume of 5Fe–5Co/ZSM-5 catalyst was reduced by approximately 13% after Fe and Co loading due to partial blockages of metal clusters, which led to this lower specific surface area. The morphology of 5Fe–5Co/ZSM-5 catalyst, examined by FE-SEM (Fig. 3), exhibited uniform, aggregated cubic particles with a mean diameter of approximately 1.1 μm. The EDS result evidently confirmed the good distribution of iron oxide and cobalt oxide nanoclusters over the surface of ZSM-5 zeolite (Fig. 3 (inset)).

The reducibility of the catalysts was evaluated by H_2-TPR, and the reduction profiles are presented in Fig. 4. Three deconvolution peaks of reduction in the temperature range of 200–800 °C are observed in 5Fe–5Co/ZSM-5 catalyst. The first peak at lower temperature (317 °C) can be assigned to transformations of Fe_2O_3 to Fe_3O_4 and of Co_3O_4 to CoO.[5,6,12] The second peak (414 °C) is attributed to the reduction of Fe_3O_4 and FeO to metallic Fe and of CoO to metallic Co, while the last peak (452 °C) can be ascribed to the reduction of remaining FeO or of hardly reducible Fe species.[7,29]

In situ XANES technique was applied to confirm the transformation of Fe and Co species on 5Fe–5Co/ZSM-5 (Fig. 5). The XANES spectra in the range 50–340 °C exhibited absorption edge energy at 7127 eV, indicating the presence of Fe_2O_3 and Fe_3O_4. Increasing the reduction temperature to above 340 °C

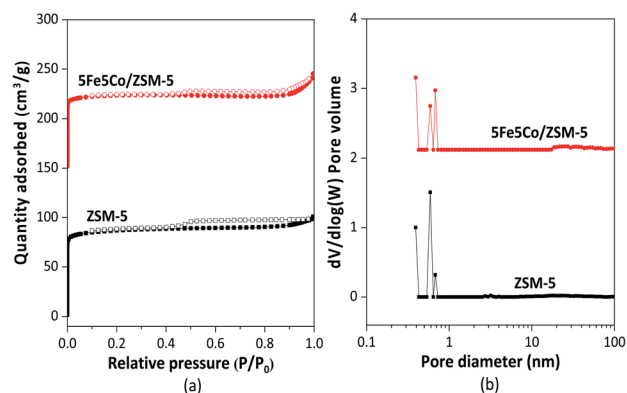Fig. 2 N_2 adsorption–desorption isotherm (a) and pore size distribution (b) of ZSM-5 support and 5Fe–5Co/ZSM-5 catalyst.

under a flow of H_2, a gradual shift of the absorption edge energy towards lower energy was observed, indicating the reduction of oxidation state of Fe species. In the case of Co species, the reduction of oxidation state occurred when increasing the reduction temperature to those higher than 300 °C. In order to determine the evolution of the oxidation states of Fe and Co species on ZSM-5 support, linear combination fitting was performed on each XANES spectrum at the reduction temperature of 400 °C, and compared to the XANES spectra of the references consisting Fe_2O_3, Fe_3O_4, FeO and Fe for Fe species, as well as Co_3O_4, CoO and Co for Co species. As shown in Fig. 6, the metal oxide catalysts were transformed to approximately 20% FeO and 70% Fe, and approximately 20% CoO and 80% Co, after the reduction process.

The magnetic properties of 5Fe–5Co/ZSM-5 catalyst before and after the reduction process at 400 °C were investigated using a vibrating sample magnetometer (VSM) (Fig. 7). Before the reduction process, 5Fe–5Co/ZSM-5 catalyst exhibited a small magnetic hysteresis loop, indicating paramagnetic nature of the catalyst.[30,31] After the reduction process, a narrower hysteresis loop was clearly observed. The saturation (M_s) and remanence
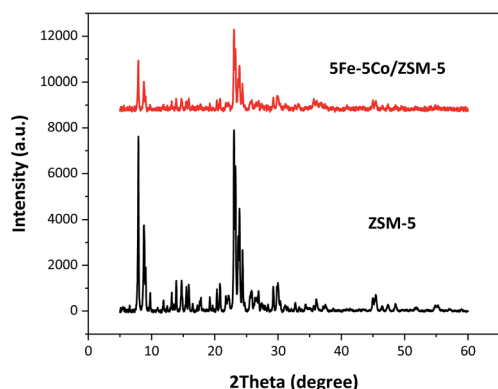

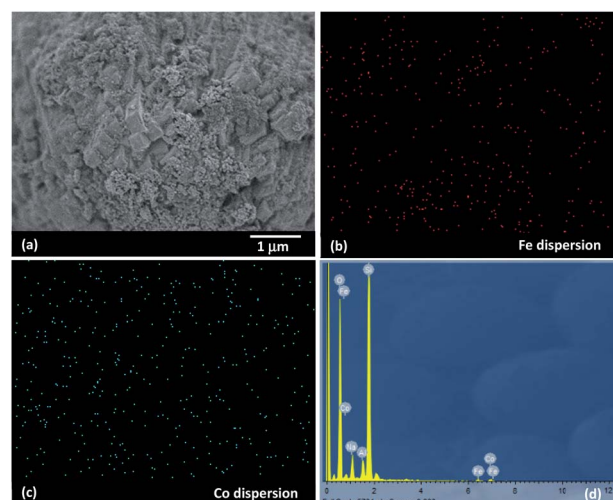Fig. 1 XRD patterns of ZSM-5 support and 5Fe–5Co/ZSM-5 catalyst.

Fig. 3 SEM images of 5Fe–5Co/ZSM-5 catalyst (a) with EDS mapping of Fe (b), Co (c) dispersions and EDS spectrum (d).
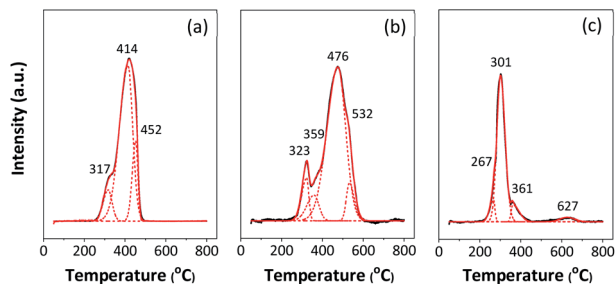
Fig. 4 H_2-TPR profile of (a) 5Fe–5Co/ZSM-5, (b) 5Fe/ZSM-5 and (c) 5Co/ZSM-5 catalysts. — TPR profile (experiment); — TPR profile (program); ---- deconvoluted profile of Fe and Cu oxide species.
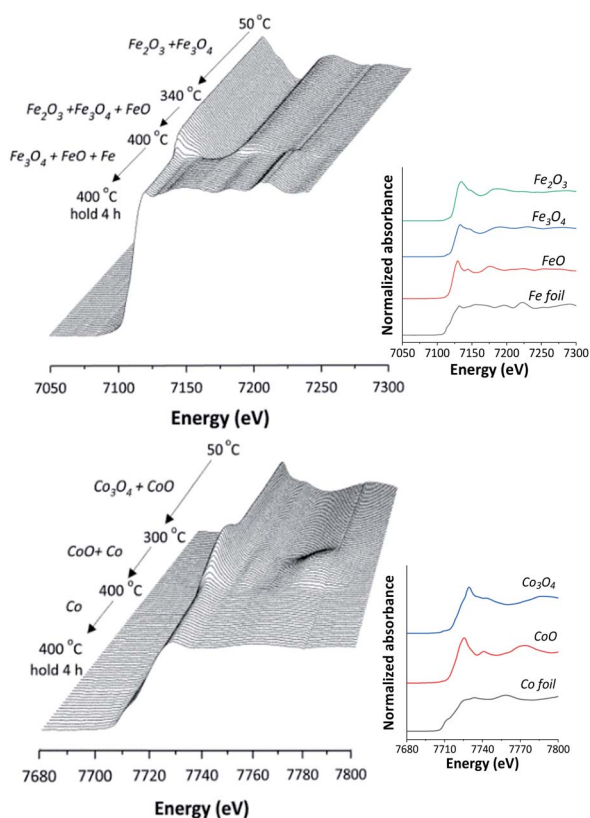

Fig. 5 *In situ* Fe K-edge and Co K-edge XANES spectra of 5Fe–5Co/ZSM-5 catalyst reduction from 50–400 °C and for 4 h holding time.

Fig. 6 Evolution of Fe and Co species during the reduction of 5Fe–5Co/ZSM-5 catalyst.

0–27.7 mT (the geomagnetic field thereby being approx. 0.03–0.06 mT). It was found that CO conversion under external magnetic field increased by a factor of 1.9 compared to that without magnetic field. Compared to the reaction over Co/Al$_2$O$_3$ catalyst, CO conversion at 15 mT increased by a factor of 1.1.[19] However, the CO conversion showed no significant variation using magnetic flux intensities ranging from 20.8–27.4 mT.

It was noted that methane yield significantly increased, while CO$_2$ obviously decreased with increasing magnetic flux intensities in the range of 0–27.4 mT. These results indicated that the external magnetic field facilitated the activity of 5Fe–5Co/ZSM-5 catalyst through increasing the reverse water–gas shift reaction.[32] This may attributed to the effective diffusion of reactant molecules and their interaction with the catalyst surface under magnetic field.

Based on the above results, it was suggested that the selective CO conversion and product selectivities under external

(M_r) magnetizations of the reduced 5Fe–5Co/ZSM-5 catalyst both significantly increased, indicating higher magnetic responses compared to the unreduced catalyst due to the existence of α-Fe phase with ferromagnetic property within the catalyst. In addition, a higher saturation magnetization of 19.0 emu g^{-1} was observed on the reduced catalyst, compared to 3.6 emu g^{-1} for the catalyst before reduction.

The performances of 5Fe–5Co/ZSM-5 catalyst in CO hydrogenation reaction were examined using a magnetic field-assisted packed bed reactor operated at 320 °C and 10 bar with a total flow rate of 30 ml min^{-1}; the results are shown in Fig. 8 and 9. Magnetic flux intensities were varied in the range of
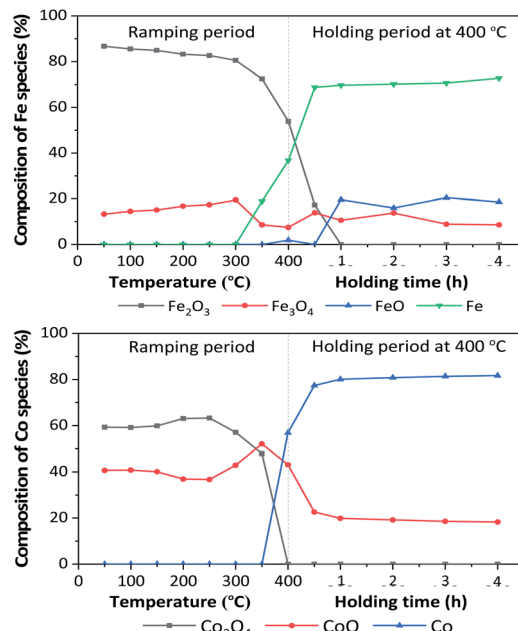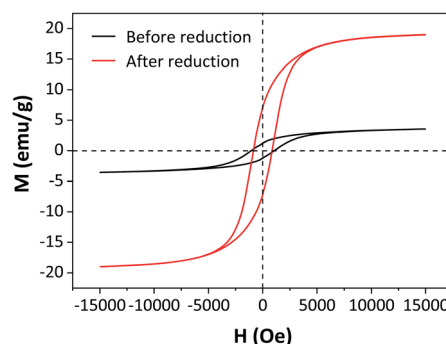

Fig. 7 Magnetic hysteresis loops of 5Fe–5Co/ZSM-5 catalyst before and after reduction process at 400 °C.
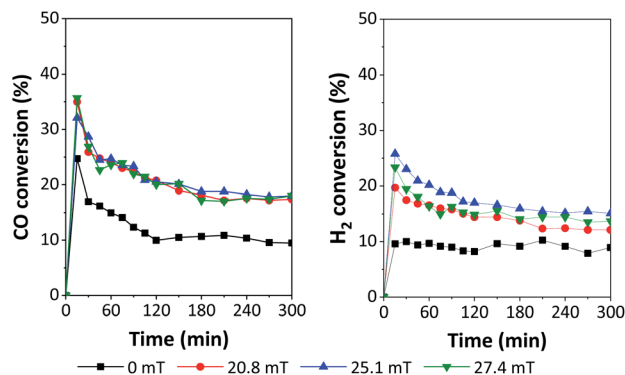
Fig. 8 Catalytic performances in terms of H₂ and CO conversion over 5Fe–5Co/ZSM-5 using different magnetic flux intensities.
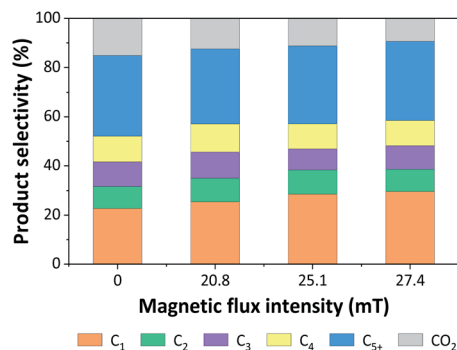

Fig. 9 Product distributions from CO hydrogenation over 5Fe–5Co/ZSM-5 catalyst for different magnetic flux intensities.

magnetic field could possibly rely not only on the improvement of catalyst active surfaces, but also on the diffusion rate of the reactants into and the product gases from the confined-space ZSM-5 zeolite based catalyst. In order to confirm the synergistic effect of the external magnetic field and limited mass transfer within zeolite cavities, the diffusion of CO and H₂ reactant molecules through 5Fe–5Co/ZSM-5 catalyst bed under external magnetic field were observed and compared to that without magnetic field, as shown in Fig. 10.

As shown in Fig. 10, the diffusion rates of both CO and H₂ reactant gases were significantly lowered principally due to the interaction with –OH functional group on ZSM-5 zeolite surfaces and limited mass transfer within zeolite cavities
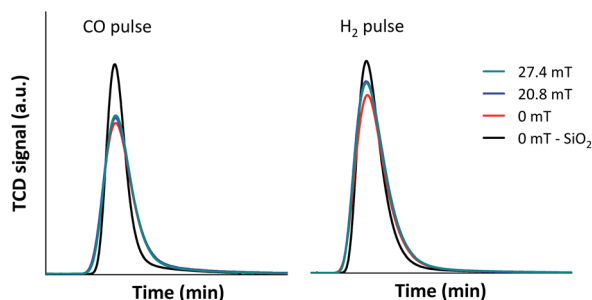

Fig. 10 CO and H₂ diffusion over 5Fe–5Co/ZSM-5 catalyst at 50 °C.

compared to inert silica. In addition, H₂ diffusivity improved considerably, more than that of CO under external magnetic field as its kinetic diameter (289 pm) is 1.3 times smaller than that of CO (376 pm). The synergistic effect of the external magnetic field and limited mass transfer within zeolite cavities therefore led to selective CO conversion to methane and larger hydrocarbon products.

In order to understand the effect of external magnetic field on the reactant gas diffusion within the confined space catalyst, the effective diffusion coefficients (D_e) of CO and H₂ were calculated using eqn (1)–(5);[33] the results are shown in Table 1.

$$D_e = D_{pore}\varepsilon/\tau \tag{1}$$

where ε is catalyst porosity, τ is catalyst tortuosity, and D_{pore} is diffusivity of CO and H₂ in pore, which is obtained from:

$$\frac{1}{D_{pore}} = \frac{1}{D_{AB}} + \frac{1}{D_k} \tag{2}$$

where D_{AB} and D_k are bulk diffusivity (cm² s⁻¹) and Knudsen diffusivity (cm² s⁻¹), respectively. The values of D_{AB} and D_k can be calculated from the following equations:

$$D_{AB} = \frac{0.001858 T^{\frac{3}{2}}\left(\frac{1}{M_{CO}} + \frac{1}{\frac{1}{3}M_{CO} + \frac{2}{3}M_{H_2}}\right)^{1/2}}{P\sigma_{COH_2}{}^2\Omega_D} \tag{3}$$

$$D_k = 9700r\left(\frac{T}{M}\right)^{1/2} \tag{4}$$

where T is reaction temperature (K); M_{CO} and M_{H_2} are molecular weights of CO and H₂, respectively; P is total pressure (atm); σ_{COH_2} is effective collision diameter (Å); Ω_D is collision integral; and r is pore radius (cm).

The tortuosity (τ) of 5Fe–5Co/ZSM-5 catalyst in eqn (1), can be calculated by using eqn (5).[34]

$$\tau = \varepsilon \Big/ \left[1 - (1-\varepsilon)^{\frac{1}{3}}\right] \tag{5}$$

Table 1 shows that effective diffusion coefficients of CO and H₂ in pores of 5Fe–5Co/ZSM-5 catalyst under external magnetic

Table 1 Diffusivities and effective diffusion coefficients of CO and H₂ in pores of 5Fe–5Co/ZSM-5 catalyst for different magnetic flux intensities

Magnetic flux intensity (mT)	Diffusivities in pores × 10⁻³ (cm² s⁻¹)		Effective diffusion coefficient × 10⁻⁴ (cm² s⁻¹)	
	CO	H₂	CO	H₂
0	0.89	3.30	4.29	15.97
20.8	1.75	4.83	8.49	23.41
25.1	2.33	9.57	11.30	46.32
27.4	1.84	6.71	8.92	32.51

field were improved by approximately 2.6 and 2.9 times, respectively, compared to those without magnetic field. This is in good agreement with the experimental results observed in Fig. 10. As a result, it can be concluded that the application of an external magnetic field to catalytic CO hydrogenation over a confined-space ZSM-5 zeolite based catalyst can facilitate the synergy between the external magnetic field and limited mass transfer within zeolite cavities. These phenomena consequently led to differences in effective diffusion abilities of CO and hydrogen during the reaction within the catalyst pores, leading to significant improvement in CO conversion.

As the reactor system consisting an external magnetic field in cooperation with a confined-space zeolite catalyst can facilitate different mass transfer abilities of reactant gases and products, the potential application for reactive separation processes by means of selective reactant and product mass transfers designed for separation—selective catalytic conversion with tailored reaction pathways are therefore able to provide a potential challenge for larger—scale green and sustainable chemical processes in the future.

Conclusions

In this work, the external magnetic field was applied for the first time for catalytic CO hydrogenation in a conventional reactor packed with a confined-space 5Fe–5Co/ZSM-5 catalyst. It was found that magnetic flux intensities at the catalyst bed in the range of -20.8 and -25.1 mT with magnetic field orientation of N–S alignment could successfully promote the CO conversion and CH_4 selectivity by factors of 1.9 and 1.3 compared to those without magnetic field, respectively. In addition, the observation on CO and H_2 diffusivies over the 5Fe–5Co/ZSM-5 catalyst evidently confirmed the synergistic effect between magnetic field and limited mass transfer within zeolite cavities as external magnetic field could promote mass transfer ability and enhance the catalytic activity with tailored reaction pathways. As a result, the concepts of magnetic field-assisted confined-space catalyst utilization are therefore able to provide an innovation challenge for green and sustainable chemical processes and separation processes by means of selective reactant and product mass transfers designed for selective catalytic conversion–separation in the future.

Conflicts of interest

There are no conflicts to declare.

Acknowledgements

References

1 H. Li, J. Wang, C. Chen, L. Jia, B. Hou and D. Li, *RSC Adv.*, 2017, **7**, 9436–9445.

2 C. I. Méndez and J. Ancheyta, *Catal. Today*, 2020, **353**, 3–16.

3 Z. Qi, L. Chen, S. Zhang, J. Sub and G. A. Somorjai, *Appl. Catal. Gen.*, 2020, **602**, 117607.

4 W. Li, H. Wang, X. Jiang, J. Zhu, Z. Liu, X. Guo and C. Song, *RSC Adv.*, 2018, **8**, 7651–7669.

5 H. Dong, M. Xie, J. Xu, M. Li, L. Peng, X. Guo and W. Ding, *Chem. Commun.*, 2011, **47**, 4019–4021.

6 V. Benedetti, S. S. Ail, F. Patuzzi, D. Cristofori, R. Rauch and M. Baratieri, *Renewable Energy*, 2020, **147**, 884–894.

7 T. Numpilai, N. Chanlek, Y. Poo-Arporn, S. Wannapaiboon, C. K. Cheng, N. Siri-Nguan, T. Sornchamni, P. Kongkachuichay, M. Chareonpanich, G. Rupprechter, J. Limtrakulg and i Witoon, *Appl. Surf. Sci.*, 2019, **483**, 581–592.

8 H. Song, Q. Zhao, X. Zhou, Z. Cao and M. Luo, *Fuel*, 2018, **229**, 144–150.

9 B. Gu, A. Y. Khodakov and V. V. Ordomsky, *Chem. Commun.*, 2018, **54**, 2345–2348.

10 H. Becker, R. Güttel and T. Turek, *Catal. Sci. Technol.*, 2016, **6**, 275–287.

11 J. Wang, H. Li, D. Li, J. P. den Breejen and B. Hou, *RSC Adv.*, 2015, **5**, 65358–65364.

12 A. Carvalho, M. Marinova, N. Batalha, N. R. Marcilio, A. Y. Khodakov and V. V. Ordomsky, *Catal. Sci. Technol.*, 2017, **7**, 5019–5027.

13 H. X. Vu, M. Schneider, U. Bentrup, T. T. Dang, B. M. Q. Phan, D. A. Nguyen, U. Armbruster and A. Martin, *Ind. Eng. Chem. Res.*, 2015, **54**(6), 1773–1782.

14 R. Liu, Z. Ma, J. D. Sears, M. Juneau, M. L. Neidig and M. D. Porosoff, *J. CO2 Util.*, 2020, **41**, 101290.

15 C. Liu, Y. Chen, Y. Zhao, S. Lyu, L. Wei, X. Li, Y. Zhang and Ji. Li, *Fuel*, 2020, **263**, 116619.

16 G. H Yao, F. Wang, X. B Wang and K. T Gui, *Energy*, 2010, **35**, 2295–2300.

17 W. Zhang, X. Wang and X. Fu, *Chem. Commu.*, 2003, 2196–2197.

18 A. N. Pour, J. Karimi, S. Taghipoor, M. Gholizadeh and M. Hashemian, *J. Iran Chem. Soc.*, 2017, **14**, 1477–1488.

19 P. Nikparsa, A. Nikparsa and A. Mirzaei, *Phys. Chem. Res.*, 2020, **8**, 645–656.

20 J. Li, L. Zhou, Q. Zhu and H. Li, *Ind. Eng. Chem. Res.*, 2013, **52**, 6647–6654.

21 J. Li, J. Li, Q. Zhu and H. Li, *Chem. Eng. J.*, 2018, **350**, 496–506.

22 B. Stuyven, Q. Chen, W. V. de Moortel, H. Lipkens, B. Caerts, A. Aerts, L. Giebeler, B. Van Eerdenbrugh, P. Augustijns, G. Van den Mooter, J. Van Humbeeck, J. Vanacken, V. V. Moshchalkov, J. Vermant and J. A. Martens, *Chem. Commun.*, 2009, **47**, 47–49.

23 L. Chen, Q. Zhu, Z. Hao, T. Zhang and Z. Xie, *Int. J. Hydrogen Energy*, 2010, **35**(6), 8494–8502.

24 S. Kiatphuengporn, P. Jantaratan, J. Limtrakul and M. Chareonpanich, *Chem. Eng. J.*, 2016, **306**, 866–875.

25 S. Kiatphuengporn, W. Donphai, P. Jantaratan, N. Yigit, K. Föttinger, G. Rupprechter and M. Chareonpanich, *J. Clean. Prod.*, 2017, **142**, 1222–1233.

26 W. Umchoo, C. Sriakkarin, W. Donphai, C. Warakulwit, Y. Poo-arporn, P. Jantaratana, T. Witoon and M. Chareonpanich, *Energ. Convers. Manage.*, 2018, **159**, 342–352.

27 B. Liu, Q. Duan, C. Li, Z. Zhu, H. Xi and Y. Qian, *New J. Chem.*, 2014, **38**, 4380–4387.

28 W. Wannapakdee, C. Wattanakit, V. Paluka, T. Yutthalekha and J. Limtrakul, *RSC Adv.*, 2016, **6**, 2875–2881.

29 L. Niu, X. Liu, X. Wen, Y. Yang, J. Xu and Y. Li, *Catal. Today*, 2020, **343**, 101–111.

30 C. Sriakkarin, W. Umchoo, W. Donphai, Y. Poo-arporn and M. Chareonpanich, *Catal. Today*, 2018, **314**, 114–121.

31 W. Donphai, N. Piriyawate, T. i Witoon, P. Jantaratana, V. Varabuntoonvit and M. Chareonpanich, *J. CO2 Util*, 2016, **16**, 204–211.

32 K. Oshima, T. Shinagawa, Y. Nogami, R. Manabe, S. Ogo and Y. Sekine, *Catal. Today*, 2014, **232**, 27–32.

33 W. L. McCabe, J. C. Smith and P. Harriott, *Unit Operations of Chemical Engineering*, McGraw-Hill, New York, 7th edn, 2005.

34 J. W. Beeckman, *Chem. Eng. Sci.*, 1990, **45**, 2603–2610.